

Hierarchical MnO₂ nanosheets synthesized via electrodeposition-hydrothermal method for supercapacitor electrodes

Dongdong Zheng^{1,2} · Yujie Qiang^{1,2} · Shenyong Xu¹ · Wenpo Li^{1,2} · Shanshan Yu¹ · Shengtao Zhang^{1,2}

Received: 27 June 2016 / Accepted: 25 December 2016 / Published online: 24 January 2017
© Springer-Verlag Berlin Heidelberg 2017

Abstract Metal oxides have emerged as one kind of important supercapacitor electrode materials. Herein, we report hierarchical MnO₂ nanosheets prepared of indium tin oxide (ITO) coated glass substrates via a hybrid two-step protocol, including a cathodic electrodeposition technique and a hydrothermal process. The samples are characterized by X-ray diffraction (XRD), X-ray photoelectron spectroscopy (XPS), scanning electron microscope (SEM) with energy dispersive X-ray spectroscopy (EDX), and transmission electron microscope (TEM). SEM and TEM images show that the as-synthesized MnO₂ nanosheets are hierarchical and porous, which could increase the active surface and short paths for fast ion diffusion. The results of nitrogen adsorption–desorption analysis indicate that the BET surface area of the MnO₂ nanosheets is 53.031 m² g⁻¹. Furthermore, the electrochemical properties of the MnO₂ are elucidated by cyclic voltammograms (CV), galvanostatic charge–discharge (GCD) tests, and electrochemical impedance spectroscopy (EIS) in 0.1 M Na₂SO₄ electrolyte. The electrochemical results demonstrate that the as-grown MnO₂ nanosheet exhibits an excellent specific capacitance of 335 F g⁻¹ at 0.5 A g⁻¹ when it is applied as a potential electrode material for an electrochemical supercapacitor. Additionally, the MnO₂ nanosheet electrode also presents high rate capability and good cycling stability with 91.8% retention after 1000 cycles. These excellent properties

indicate that the hierarchical MnO₂ nanosheets are a potential electrode material for electrochemical supercapacitors.

1 Introduction

Electrochemical capacitors (ECs) are also known as ultracapacitors, electrical double layer capacitors, or supercapacitors. ECs as an effective way of the energy storage have attracted considerable attention due to the properties of high power density, excellent cycle stability, and rapid charging–discharging rate [1–3]. Various materials have been investigated as the electrode materials in supercapacitors. To date, the most widely used active materials for ECs electrodes include three types, i.e. carbon materials, conducting polymers and transition metal oxides [4–9]. Metal oxides have the advantage of better cycling stability than polymer materials and own higher energy density than conventional carbon materials, but they possess a pivotal inferior of poor conductivity. Among these materials, manganese oxide (MnO₂) has attracted significant interest due to its high theoretical specific capacitance, low-cost, abundance and environmentally friendly property [10, 11]. However, the poor conductivity, slow ion transport rate and short cycle limit the specific capacitance of MnO₂ [12, 13]. Therefore, further efforts have been devoted to maximize their capabilities and electrochemical performance by incorporating nanoscale MnO₂ electrode materials with highly porous and electrically conductive materials to form hybrid or composite nanostructures [5, 14].

In order to obtain MnO₂ with the desired morphology and high accessible surface sites to achieve highest theoretical capacitance, extensive efforts have been dedicated to adjust synthesis methods, including hydrothermal synthesis [15], sol–gel process [16], electrodeposition

✉ Wenpo Li
liwenpo@aliyun.com

¹ School of Chemistry and Chemical Engineering, Chongqing University, Chongqing 400044, People's Republic of China

² National-municipal Joint Engineering Laboratory for Chemical Process Intensification and Reaction, Chongqing 400044, People's Republic of China

method [17], template method [18], and electrophoretic co-deposition [19]. According to literatures, MnO_2 has several morphologies, such as nanowires, nanorods, nanosheets, and hierarchical structures [12, 20, 21]. Among these morphologies, hierarchical materials could facilitate applications in ECs since they can provide large surface areas for reaction, interfacial transport and also shorten diffusion paths [22, 23]. For instance, Zhang et al. introduced NiCo_2O_4 into MnO_2 nanostructured electrodes to synthesize a 3D hierarchical $\text{NiCo}_2\text{O}_4@ \text{MnO}_2$ hybrid which showed a high specific capacitance of 913.6 F g^{-1} at 0.5 A g^{-1} [24]. Yu et al. fabricated hierarchical core-shell-like $\text{MnO}_2@ \text{MnO}_2$ nanoarchitectures on carbon fibers and obtained a maximum specific capacitance of 244.54 F g^{-1} at a current density of 0.5 A g^{-1} [25]. And, Liu et al. synthesized graphene nanoribbon- MnO_2 hierarchical hybrid nanomaterials exhibiting a significantly specific capacitance of 305 F g^{-1} at 0.5 A g^{-1} [26]. Since the hierarchical pore structure may result in a better performance of supercapacitors, it is necessary to develop novel hierarchical structures directly on conductive substrates using simple, convenient, and cost-effective approaches. More recently, researches have been focused on the application of a hydrogen coevolution cathodic electrodeposition followed by oxidation process for the synthesis of high surface MnO_2 films [12, 21, 27]. Manganese hydroxide ($\text{Mn}(\text{OH})_2$) can be converted to MnO_2 by an in situ electrooxidation progress [21] or annealing in the presence of oxygen [12]. Significantly, the hydrothermal process has been proved to be an effective and controllable method to produce MnO_2 with various hierarchical nanostructures [20, 28].

In this paper, we demonstrated the synthesis of hierarchical MnO_2 nanosheets through a hydrogen coevolution cathodic electrodeposition followed by a facile hydrothermal process, which was first used to convert the $\text{Mn}(\text{OH})_2$ to hierarchical MnO_2 nanosheets. The aims of designing such MnO_2 are listed as the following: (1) the MnO_2 nanosheets would relax the transport of ions because of the nanostructures. (2) The pores of the MnO_2 would enable fast, reversible Faradaic reactions and provide short ion diffusion paths. (3) The hierarchical MnO_2 would obviously enhance the utilization rate of MnO_2 material because of large specific surface area. Electrochemical measurements show that the MnO_2 nanosheets, tested as an electrode material, exhibit a higher specific capacitance (391 F g^{-1} at 5 mV s^{-1} and 335 F g^{-1} at 0.5 A g^{-1}), and a long-term cycling stability (91.8% capacitance retention after 1000 consecutive cycles). Remarkably, the as-prepared hierarchical MnO_2 films exhibit superior pseudocapacitive performance with excellent cycling stability and high-rate capacity during cycling, they are promising materials for high-performance ECs applications.

2 Experiment

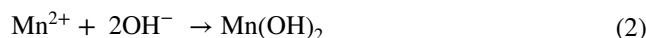
2.1 Experimental procedure

2.1.1 Materials

MnSO_4 , Na_2SO_4 , KMnO_4 , acetone (AR; Chuandong Chemical Co., Chongqing), Teflon-lined pressure vessel (Jiapeng Chemical Co., Chongqing), ITO (Sn-doped- In_2O_3 , $15 \Omega \text{ sq}^{-1}$, $10 \times 10 \text{ mm}$), and Pt foil ($10 \times 10 \text{ mm}$, 2 mm in thickness, 99.99%). All chemicals used in this work were of analytical reagent grade and used as received without further purification.

2.1.2 Preparation of $\text{Mn}(\text{OH})_2$

$\text{Mn}(\text{OH})_2$ films were electrodeposited without templates in the solution containing 0.1 M MnSO_4 and 0.1 M Na_2SO_4 at a bath temperature of 25°C . ITO with a typical area of $1 \times 1 \text{ cm}^2$ was used as cathode for the growth of $\text{Mn}(\text{OH})_2$ film, and Pt foil was used as a counter electrode. Before electrodeposition, ITO and Pt were treated with acetone to remove contaminants. The two electrodes were separated by a distance of 30 mm, and the electrodeposition was carried out by pulse current at a cathodic current density of 0.1 A dm^{-2} . The parameter included pulse interval (80 ms), on time (50 ms) and cycles (1000). The as-electrodeposited films were washed thoroughly with distilled water. The cathodic electrodeposition leads to the formation of $\text{Mn}(\text{OH})_2$ as the following reaction [12, 29, 30]:



The coevolution H_2 bubbles act as a dynamic template for the formation and growth of porous nanostructure [21] or nanosheet arrays of $\text{Mn}(\text{OH})_2$ [27].

2.1.3 Synthesis of hierarchical MnO_2 nanosheets

In the subsequent step, MnO_2 films were obtained by hydrothermal reaction using the prepared $\text{Mn}(\text{OH})_2$ films and KMnO_4 at moderate temperature in a Teflon-lined pressure vessel. Briefly, 0.44 g KMnO_4 was dissolved in 35 mL distilled water first. Subsequently, the well-mixed aqueous solution of KMnO_4 was transferred into a Teflon-lined pressure vessel with the as-deposited $\text{Mn}(\text{OH})_2$ films on ITO dipped into the vessel, sealed and heated at 110°C or 160°C for 24 h, respectively. The formation of MnO_2 is as the following reaction:



After the reaction was finished, the pressure vessel was cooled to room temperature naturally. The MnO₂ films on ITO were washed with distilled water and finally dried at 80 °C in air. In short, the synthesis of hierarchical MnO₂ nanosheets was carried out by a two-step approach of a cathodic electrodeposition followed by a hydrothermal treatment. The whole fabrication process for hierarchical MnO₂ nanosheets as supercapacitor electrode materials is illustrated in Fig. 1.

2.2 Material characterization and electrochemical test

The prepared films were characterized by X-ray photoelectron spectroscopy (XPS, ESCALab250), transmission electron microscope (TEM, JEM-100CX II), and X-ray diffractometer (XRD, XRD-6000) and scanning electron microscopy (SEM, JSM-7800F) with energy dispersive X-ray spectroscopy (EDX). And, Nitrogen adsorption-desorption isotherms were measured at 77 K on Quadrasorb SI system. Specific surface area and pore volume were calculated by the Brunauer-Emmett-Teller (BET) method. Pore size distribution was estimated from desorption branches of isotherms by the Barrett, Joyner, and Halenda (BJH) method. In addition, inductively coupled plasma atomic emission spectroscopy (ICP, ICAP6300) was used to analyze the actual loading of MnO₂ on the conductive substrates.

The electrochemical properties of the MnO₂ films were investigated with a CHI660B electrochemical workstation (Chenhua, Shanghai) under cyclic voltammetry (CV), Galvanostatic charge-discharge (GCD) tests, and electrochemical impedance spectroscopy (EIS) measurements in a conventional three-electrode cell. The three-electrode cell configuration consisted of a Pt foil as the counter electrode, a standard calomel electrode (SCE) as the reference electrode, and the products prepared on ITO substrates as the working electrode. A solution containing 0.1 M Na₂SO₄ served as the electrolyte at 25 °C. CVs were recorded between 0 and 0.8 V vs. SCE at various scan rates ranging from 5 to 100 mV s⁻¹. GCD testing was conducted between 0 and 0.8 V vs. SCE. Then EIS measurements were carried out at the frequencies from 100 kHz to 0.01 Hz.

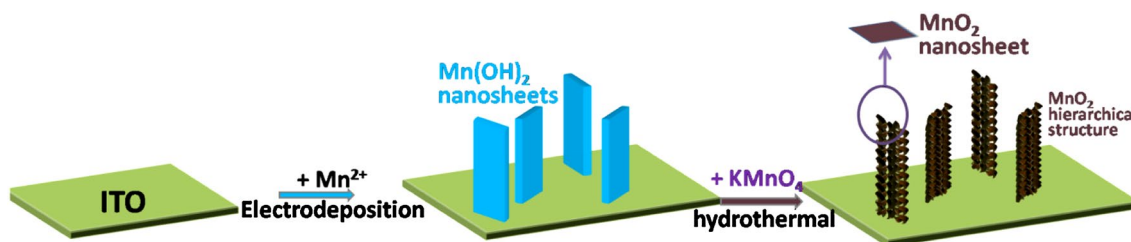


Fig. 1 Schematic illustration of the fabrication processes for hierarchical MnO₂ nanosheets

3 Results and discussion

Figure 2 shows the XRD patterns of prepared Mn(OH)₂ by cathodic electrodeposition. Excluding strong peaks from In₂O₃ (JCPDS card no.06-0416), the weaker diffraction peaks Mn(OH)₂ (JCPDS card no. 08-0171) are observed. Since Mn(OH)₂ is easily oxidized in air and affected by strong signal from In₂O₃, there is lack of clear peaks. The XRD patterns suggest that the sample is in poor crystalline state.

In Fig. 3a, EDX analyses revealed that the MnO₂ film consisted of manganese and oxygen, and no other chemical elements were detected except elements of ITO substrate. XPS for the MnO₂ film is given in Fig. 3b. The binding energy peaks of 2p_{3/2} and 2p_{1/2} are located at 642.3 eV and 653.9 eV, respectively, which can be assigned to Mn2p_{3/2} and Mn2p_{1/2} of Mn⁴⁺ in pure MnO₂ [27, 31]. Figure 3c shows the XRD pattern of the MnO₂ film on the substrate. There are several peaks assigned to In₂O₃ in ITO substrate. A careful examination of all the manganese oxide XRD patterns enabled us to find out that the chemical compound was most likely ε-MnO₂ (JCPDS card no. 12-0141) which has low crystallinity and that the peaks could not be indexed. Therefore, EDX, XPS, and XRD analyses jointly indicated that the prepared MnO₂ films consisted of

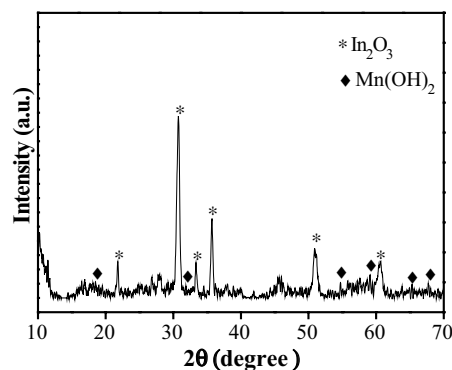


Fig. 2 XRD patterns of prepared Mn(OH)₂ by cathodic electrodeposition

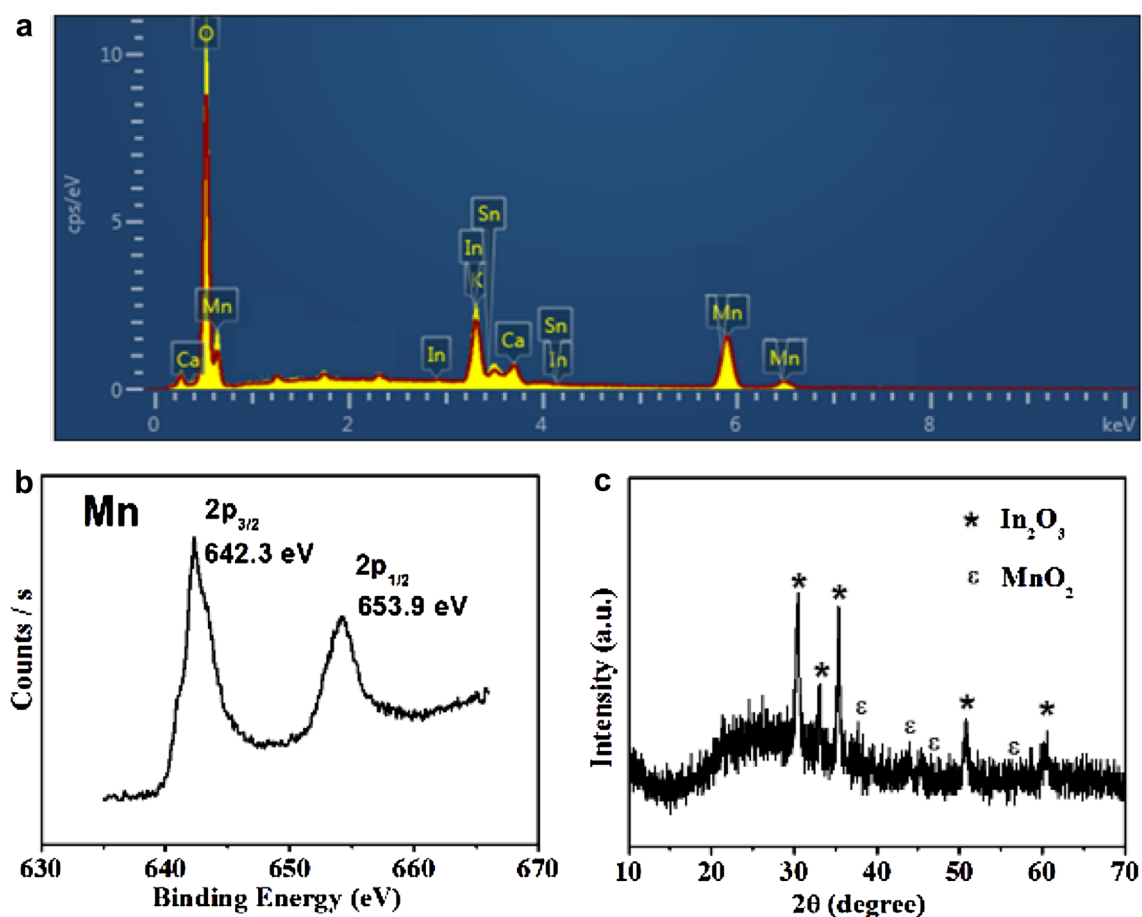
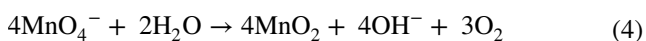


Fig. 3 a EDX, b XPS of Mn2p, and c XRD of obtained MnO₂ films at 110°C

manganese dioxide without appreciable impurity of other elements.

Figure 4a shows the morphology of the as-electrodeposited Mn(OH)₂ without hydrothermal oxidation. It can be seen that as-electrodeposited Mn(OH)₂ has free-standing and homogeneous nanosheet array structure with highly uniform surface, which are consistent with the previous reports [27]. In the homogeneous nanosheet arrays, the nanosheet thickness varied from 20 to 50 nm. Figure 4b shows SEM image of the synthesized MnO₂ film after hydrothermal oxidation at 110°C. This MnO₂ is presented as thick MnO₂ sheets with an average thickness of 80 nm, which consisted of developing nanosheets on its surface. Compared with Mn(OH)₂ nanosheets (Fig. 4a), the hierarchical MnO₂ sheets also freely stand on ITO substrate, but the thickness of MnO₂ nanosheets increased and the surface changed. As showed in Fig. 4c, compared with Fig. 4b, the MnO₂ possesses a cluster structure, possibly resulting from the self-decomposition of KMnO₄ at 160°C. The hydrothermal reaction of the decomposition of KMnO₄ can be expressed as [32]:



Clearly, there is no hierarchical structure compared with the SEM image of obtained MnO₂ at 110°C. The hierarchical MnO₂ sheets were also observed by TEM image at 110°C in Fig. 4d. TEM observation further reveals that the uniform MnO₂ sheets are assembled by MnO₂ nanosheets with a thickness of 2–4 nm. The desirable porous structure on MnO₂ sheets surface was obtained due to the random self-assembling and the unparallel nanosheets [33]. The unique hierarchical MnO₂ nanosheets are different from that of hollow sea-urchin shaped MnO₂ hierarchical nanostructures which were prepared *via* the hydrothermal reduction of KMnO₄ [28, 34]. The nanopores could afford high specific surface area for electrochemical energy storage and decrease the electrolyte ion transportation path. Consequently the hierarchical porous structure is in favor of the enhancement of supercapacitors performance [35].

The mass of MnO₂ was obtained by ICP [36]. Figure 5a illustrates a comparison of CV curves of the MnO₂ nanosheets at 110°C and 160°C at a fixed scan rate of 20 mV s⁻¹. The shape of CV curve at 110°C presents typical pseudocapacitive behavior. The area of the CV curves is directly proportional to the charge, and is

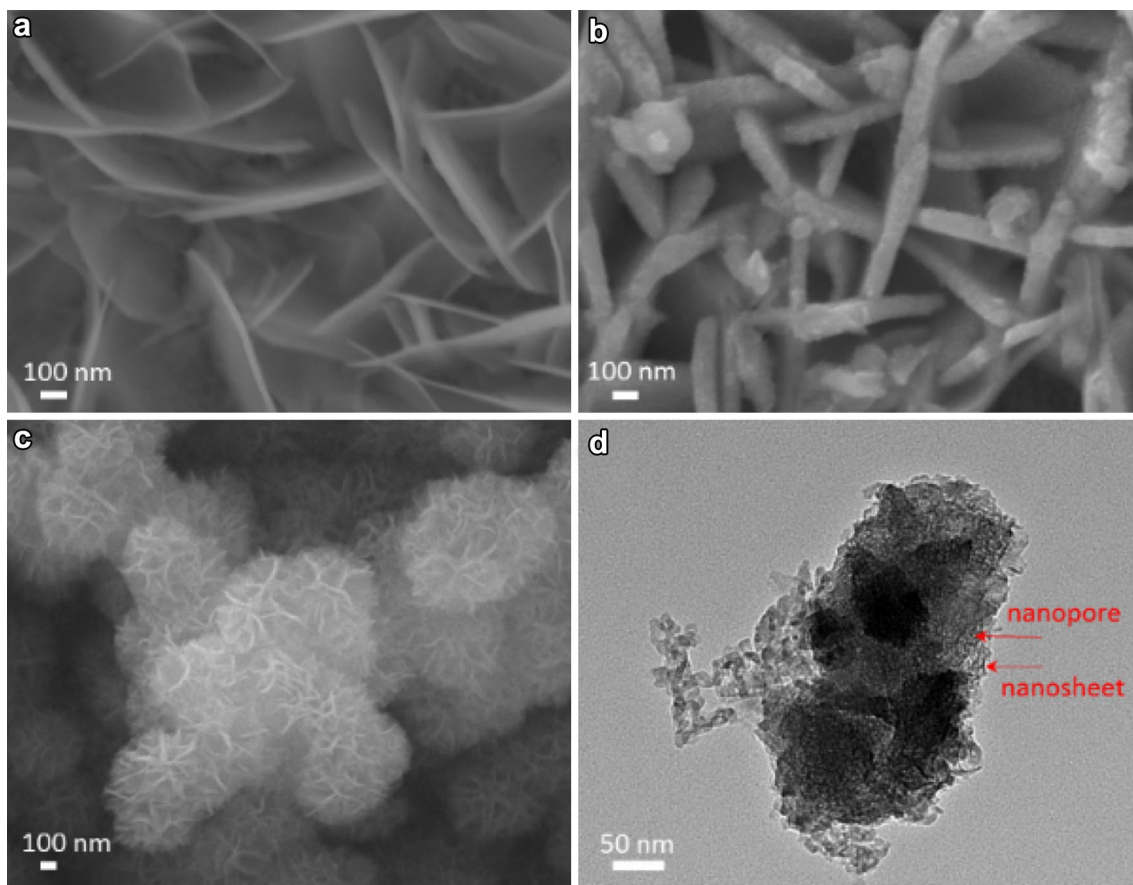


Fig. 4 SEM images of (a) the as-electrodeposited Mn(OH)₂, the obtained MnO₂ at (b) 110°C, (c) 160°C, and (d) TEM image of the obtained MnO₂ after hydrothermal oxidation at 110°C

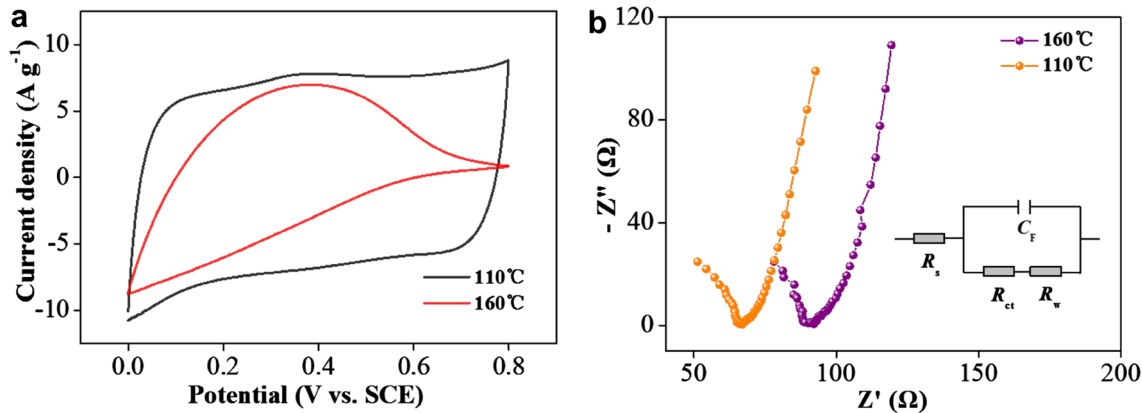


Fig. 5 a Cyclic voltammograms at 110°C and 160°C and b Nyquist plots for MnO₂ electrodes at the frequencies from 100 kHz to 0.01 Hz at 110°C and 160°C. The inset shows the equivalent circuit

finally proportional to the capacitance [37]. EIS analysis is employed to further gain a deep insight into the electrochemical properties of hierarchical MnO₂ nanosheet electrodes. Figure 5b compares Nyquist impedance spectra for the MnO₂ prepared at different temperatures. It can

be found that the Nyquist plots consist of semicircle arcs at high frequency and straight lines at low frequency. It is widely acknowledged that the semicircle presents the electrochemical reaction impedance of the film electrode and the straight line displays the diffusion of the electroactive

species [38]. A bigger semicircle means larger charge-transfer resistance, and higher slope indicates higher diffusion rate. The inset of the equivalent circuit fitting the impedance curve of the MnO_2 is displayed in Fig. 5b, where the R_s is the bulk electrolyte resistance, R_{ct} is Faradic charge-transfer resistance, R_w is the ion diffusion resistance in electrolyte, and C_F is the electrochemical capacitance. The comparison chart illustrates that the MnO_2 at 110°C has a smaller R_{ct} than 160°C and the MnO_2 at 110°C has a straight slopping line, meaning that it has a smaller R_w , leading to a better electrochemical character than the MnO_2 at 160°C . Clearly, we could draw a conclusion that MnO_2 nanosheets at 110°C have superior specific capacitance value. Therefore, the temperature of 110°C is the suitable temperature to synthesize the MnO_2 nanosheets.

Figure 6 presents the Nitrogen adsorption–desorption isotherms and pore size distribution for the MnO_2 nanosheets hydrothermally oxidated at 110°C . BET surface area measurement reveals that the MnO_2 nanosheets have a BET surface area of $53.031\text{ m}^2\text{ g}^{-1}$, much larger than the previous reports [20, 34]. The pore size distribution, calculated from the adsorption branch of the nitrogen sorption isotherm, reveals that the average pore size is $\sim 2.0\text{ nm}$. Such unique MnO_2 nanosheet arrays with high specific surface area could provide large active sites and fast charge transfers at electrode–electrolyte interface, ensuring the high electrochemical capacity for the MnO_2 nanosheets electrode.

To explore the advantages of MnO_2 hydrothermally oxidated at 110°C as electrodes for ECs, we studied their performance by performing CV measurements, GCD tests, and EIS. Figure 7a shows the CV curves of the MnO_2 electrode in $0.1\text{ M Na}_2\text{SO}_4$ at different scan rates ($5\text{--}100\text{ mV s}^{-1}$). The shape of CV curves is close to a well-defined rectangular within the potential range of $0\text{--}0.8\text{ V}$, indicating the ideal electrical double-layer capacitance behavior and fast

charging–discharging process characteristic. As the scan rate increases, the shape of the CV curves remains unchanged, demonstrating an excellent rate capacitive performance [39, 40]. The specific capacitance (F g^{-1}) was calculated from CV curve at different scan rates using the following equation [41]:

$$C_s = \frac{\int I dv}{m \cdot v \cdot \Delta V}, \quad (5)$$

where I is the response current (A), m is the mass of the MnO_2 (g), v is the scan rate of CV curves (V s^{-1}), and ΔV is the potential window width (V). The specific capacitance of the MnO_2 nanosheets arrays is calculated at different scan rates and different current densities, as showed in Fig. 7d. The specific capacitance of the MnO_2 nanosheets arrays is calculated to be 391 F g^{-1} at 5 mV s^{-1} and 335 F g^{-1} at 0.5 A g^{-1} . The higher specific capacitance results from the highly porous structure which facilitates ion transfer into the MnO_2 electrode [42]. We can see the specific capacitance gradually decreases with increase of the scan rates and the current densities. The decrease in capacitance suggests that parts of the surface of the electrode are inaccessible at high scan rates. In that case, the Na^+ ion will have difficulty in permeating into the bulk of the electrode at high scan rates, causing the reduced diffusion time. Furthermore, the material in the deep pore has little impact on the pseudocapacitance [43–45].

GCD curves of MnO_2 were further measured as shown in Fig. 7b. A high linear and symmetric nature is observed, illustrating a better electrochemical capacitive characteristic and superior reversible redox reaction between alkali cations (Na^+) and the MnO_2 nanosheets [33]. The specific capacitance is calculated according to the following equation [46]:

$$C_s = \frac{I \cdot \Delta t}{m \cdot \Delta V}. \quad (6)$$

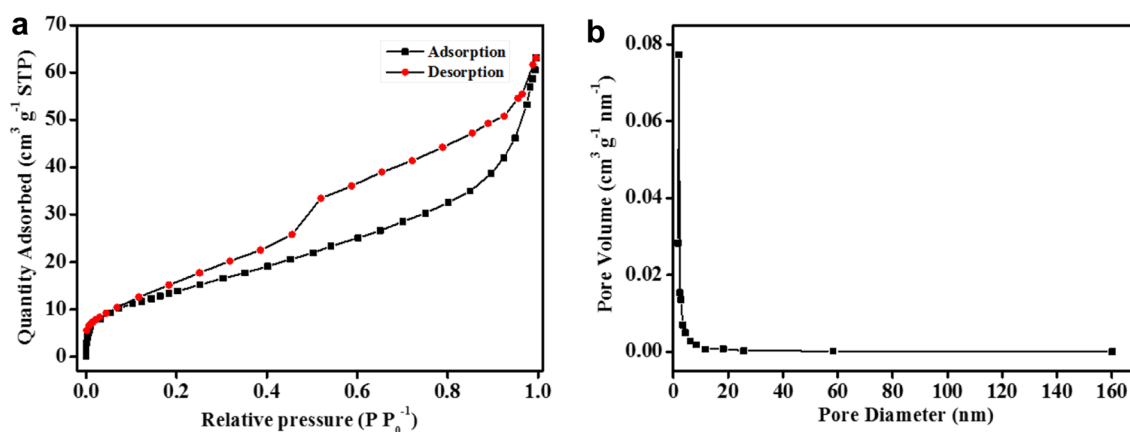


Fig. 6 Nitrogen adsorption–desorption isotherms (a) and the pore size distribution curve from the adsorption branch (b) of the MnO_2 nanosheets hydrothermally oxidated at 110°C

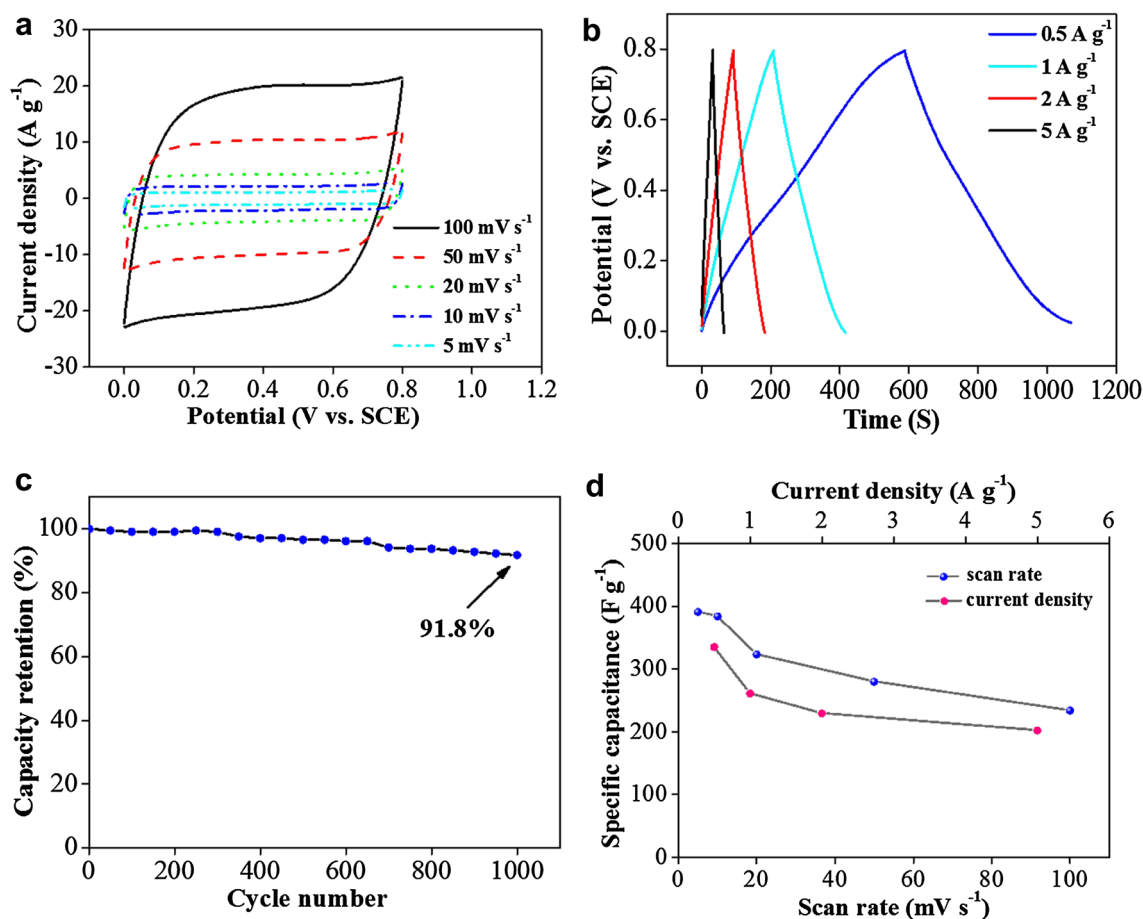


Fig. 7 **a** CV curves of the hierarchical MnO₂ nanosheets at different scan rates, **b** GCD curves of the hierarchical MnO₂ nanosheets at different current densities, **c** cycle performance of the hierarchical MnO₂

nanosheets, and **d** the specific capacitance of MnO₂ at different scan rates and different current densities

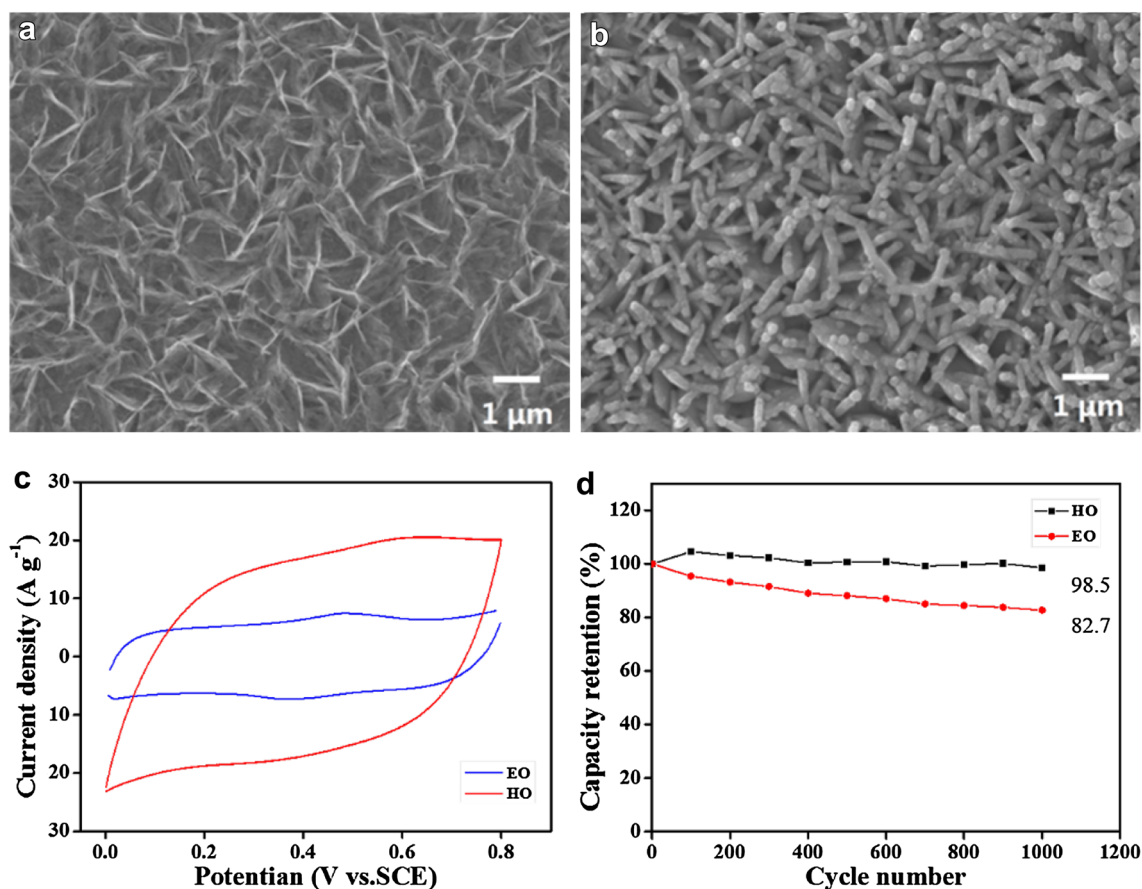
where I is the discharge current (A), Δt is the discharge time (s), m is the mass of MnO₂ (g), and ΔV is the potential drop (V) during the discharging. The specific capacitances are calculated from the galvanostatic discharge processes at current densities of 0.5, 1, 2, and 5 A g⁻¹ are 335, 261, 229, and 202 F g⁻¹, respectively; and the C_s retention ratio is 77.2% when the current density is increased 10 times to 5 A g⁻¹. The noticeable improvement of the specific capacitance of MnO₂ film is attributed to the unique hierarchical porous architecture which could shorten diffusion paths for electrolyte ions, significantly enhancing the intercalation of ions and the utilization rate of electrode material. The hierarchical MnO₂ nanosheets can provide larger surface area for more available electroactive sites. Moreover, the nanopores are able to absorb the electrolyte and shorten the diffusion paths, assuring efficient contact between active materials and electrolytes [35]. However, the capacity decreases with the increase in applied current density, which was caused by the combination of large voltage (IR) drop and distributed resistance of the pores [19, 47].

Excellent cycling stability is vital for EC operations. Herein, the long-term cycle stability of MnO₂ nanosheets electrode is evaluated by repeating the charging–discharging test at a current density of 5 A g⁻¹ for 1000 cycles, as presented in Fig. 7c. After 1000 consecutive cycles, the discharge capacitance maintains at around 91.8% of the initial value, showing a higher electrochemical cycling stability. Table 1 shows the electrochemical properties of the as-synthesized hierarchical MnO₂ nanosheets and the recent reported data in the literature for comparison purposes. It can be seen that the higher capacitance and improved cycling stability are attributed to the hierarchically porous structure, which could hinder the corruption of MnO₂ more validly [48].

To get more information of the synthesized MnO₂ films, Fig. 8 is presented to compare the MnO₂ after electrochemical oxidation (EO) (Fig. 8a) and hydrothermal oxidation (HO) at 110 °C (Fig. 8b). Figure 8a has an inhomogeneous and unordered MnO₂ film, which can result in high ion transport resistance and decrease the

Table 1 Comparison of the electrochemical properties between the as-synthesized hierarchical MnO₂ nanosheets and the recent reported data in the literature

Electrode materials	Electrolyte	Specific capacitance	Stability (cycles)	Refs.
NiCo ₂ O ₄ @MnO ₂ nanosheet networks	1 M KOH	913.6 F g ⁻¹ at 0.5 A g ⁻¹	87.1% (3000)	[24]
α-MnO ₂ nanowires@ultrathin δ-MnO ₂ nanosheets	6 M KOH	153.8 F g ⁻¹ at 20 A g ⁻¹	98.1% (10,000)	[16]
Graphite/PEDOT/MnO ₂ composites	0.5 M Na ₂ SO ₄	195.7 F g ⁻¹ at 0.5 A g ⁻¹	81.1% (2000)	[49]
Core-shell-like MnO ₂ @MnO ₂ nanoarchitectures	1 M Na ₂ SO ₄	244.54 F g ⁻¹ at 0.5 A g ⁻¹	220.4% (5000)	[25]
Graphene/CNTs/MnO ₂ nanoneedles	1 M Na ₂ SO ₄	367.23 F g ⁻¹ at 10 mV s ⁻¹	84.6% (1000)	[50]
Graphene nanoribbon-MnO ₂ hybrids	PAAK/KCl	305 F g ⁻¹ at 0.5 A g ⁻¹	88% (5000)	[26]
MnO ₂ @PEDOT@MnO ₂ nanocomposite	0.5 M Na ₂ SO ₄	449 F g ⁻¹ at 0.5 A g ⁻¹	91.3% (5000)	[51]
MnO ₂ nanosheet/carbon fiber	1 M Na ₂ SO ₄	634.5 F g ⁻¹ at 2.5 A g ⁻¹	95.2% (3000)	[16]
Hierarchical MnO ₂ nanosheets	0.1 M Na ₂ SO ₄	335 F g ⁻¹ at 0.5 A g	91.8% (1000)	This work

**Fig. 8** SEM images of MnO₂ after (a) electrochemical oxidation (EO) and (b) hydrothermal oxidation (HO). Electrochemical properties of the MnO₂ after EO and HO: (c) CV curves and (d) the life cycle stability at 0.1 V s⁻¹

specific capacitance. As expected, the MnO₂ nanosheets after HO are uniformly deposited and homogeneously aligned on the ITO, which has a highly open and porous structure in contrast to the MnO₂ after EO. As showed in Fig. 8b, the forming porous structure can endow the fast diffusion of electrolyte ions into pores and reduce the

transport length of ions and ion transport resistance, leading to a better rate performance of supercapacitors [52]. As shown in Fig. 8c, d, the MnO₂ after HO has a higher specific capacitance and capacitance retention. Obviously, the MnO₂ after HO has a superior cycling stability and can receive higher specific capacitance.

4 Conclusions

In summary, the hierarchical MnO₂ nanosheets were synthesized through a hydrogen coevolution cathodic electrodeposition followed by a hydrothermal oxidation process. These nanosheets provide a large electrochemically active surface area for fast and reversible Faradic reaction and exhibit a specific capacitance (391 F g⁻¹ at 5 mV s⁻¹ and 335 F g⁻¹ at 0.5 A g⁻¹). Moreover, the hierarchical MnO₂ nanosheets retain 91.8% of its initial capacitance even after 1000 cycles of galvanostatic charge–discharge process. The high-performance MnO₂ nanosheets can be attributed to the highly accessible specific surface area and reduced diffusion length of ions. Such results not only demonstrated the hierarchical MnO₂ nanosheets are promising materials for supercapacitor devices, but also presented a hybrid approach for fabricating nanostructure.

Acknowledgements This work was supported by the National Natural Science Foundation of China (No. 21003163) and Central University Basic Research Funds (No. 106112013025).

References

- G. Wang, L. Zhang, J. Zhang, A review of electrode materials for electrochemical supercapacitors. *Chem. Soc. Rev.* **41**, 797–828 (2012)
- C. Shen, X. Wang, S. Li, J.G. Wang, W. Zhang, F. Kang, A high-energy-density micro supercapacitor of asymmetric MnO₂–carbon configuration by using micro-fabrication technologies. *J. Power Source* **234**, 302–309 (2013)
- P. Simon, Y. Gogotsi, B. Dunn, Where do batteries end and supercapacitors begin? *Science* **343**, 1210–1211 (2014)
- H.R. Byon, S.W. Lee, S. Chen, P.T. Hammond, Y. Shao-Horn, Thin films of carbon nanotubes and chemically reduced graphenes for electrochemical micro-capacitors. *Carbon* **49**, 457–467 (2011)
- J. Cao, X. Li, Y. Wang, F.C. Walsh, J.-H. Ouyang, D. Jia, Y. Zhou, Materials and fabrication of electrode scaffolds for deposition of MnO₂ and their true performance in supercapacitors. *J. Power Source* **293**, 657–674 (2015)
- N.L. Wu, Nanocrystalline oxide supercapacitors. *Mater. Chem. Phys.* **75**, 6–11 (2002)
- T. Brousse, M. Toupin, D. Bélanger, A hybrid activated carbon-manganese dioxide capacitor using a mild aqueous electrolyte. *J. Electrochem. Soc.* **151**, A614 (2004)
- T. Cottineau, M. Toupin, T. Delahaye, T. Brousse, D. Bélanger, Nanostructured transition metal oxides for aqueous hybrid electrochemical supercapacitors. *Appl. Phys. A* **82**, 599–606 (2005)
- Y. Zhang, X. Cao, Z. Li, D. Zhao, Co-assembly of functional graphene and multiwall carbon nanotubes for supercapacitors by a vertical deposition technique. *Appl. Phys. A* **122**, 1–7 (2016)
- W. Wei, X. Cui, W. Chen, D.G. Ivey, Manganese oxide-based materials as electrochemical supercapacitor electrodes. *Chem. Soc. Rev.* **40**, 1697–1721 (2011)
- M. Huang, R. Mi, H. Liu, F. Li, X.L. Zhao, W. Zhang, S.X. He, Y.X. Zhang, Layered manganese oxides-decorated and nickel foam-supported carbon nanotubes as advanced binder-free supercapacitor electrodes. *J. Power Source* **269**, 760–767 (2014)
- T. Yousefi, A.N. Golikand, M. Hossein Mashhadizadeh, M. Aghazadeh, Facile synthesis of α -MnO₂ one-dimensional (1D) nanostructure and energy storage ability studies. *J. Solid State Chem.* **190**, 202–207 (2012)
- Z. Yu, B. Duong, D. Abbitt, J. Thomas, Highly ordered MnO₂ nanopillars for enhanced supercapacitor performance. *Adv. Mater.* **25**, 3302–3306 (2013)
- J.G. Wang, F.Y. Kang, B.Q. Wei, Engineering of MnO₂-based nanocomposites for high-performance supercapacitors. *Prog. Mater. Sci.* **74**, 51–124 (2015)
- D. Su, H.J. Ahn, G. Wang, Hydrothermal synthesis of α -MnO₂ and β -MnO₂ nanorods as high capacity cathode materials for sodium ion batteries. *J. Mater. Chem. A* **1**, 4845–4850 (2013)
- N. Yu, H. Yin, W. Zhang, Y. Liu, Z.Y. Tang, M.Q. Zhu, High-performance fiber-shaped all-solid-state asymmetric supercapacitors based on ultrathin MnO₂ nanosheet/carbon fiber cathodes for wearable electronics. *Adv. Energy Mater.* **6**, 1501458 (2016)
- S. Chou, F. Cheng, J. Chen, Electrodeposition synthesis and electrochemical properties of nanostructured γ -MnO₂ films. *J. Power Source* **162**, 727–734 (2006)
- R. Liu, S.B. Lee, MnO₂/poly(3,4-ethylenedioxythiophene) coaxial nanowires by one-step coelectrodeposition for electrochemical energy storage. *J. Am. Chem. Soc.* **130**, 2942–2943 (2008)
- R. Ranjusha, S. Ramakrishna, A.S. Nair, P. Anjali, S. Vineeth, T.S. Sonia, N. Sivakumar, K.R.V. Subramanian, S.V. Nair, A. Balakrishnan, Fabrication and performance evaluation of button cell supercapacitors based on MnO₂ nanowire/carbon nanobead electrodes. *RSC Adv.* **3**, 17492 (2013)
- Y. Huang, Y.Y. Li, Z.Q. Hu, G.M. Wei, J.L. Guo, J.P. Liu, A carbon modified MnO₂ nanosheet array as a stable high-capacitance supercapacitor electrode. *J. Mater. Chem. A* **1**, 9809–9813 (2013)
- W. Xiao, H. Xia, J.-Y.-H. Fuh, L. Lu, Electrochemical synthesis and supercapacitive properties of ϵ -MnO₂ with porous/nanoflaky hierarchical architectures. *J. Electrochem. Soc.* **156**, A627 (2009)
- Z. Chen, Y. Qin, D. Weng, Q. Xiao, Y. Peng, X. Wang, H. Li, F. Wei, Y. Lu, Design and synthesis of hierarchical nanowire composites for electrochemical energy storage. *Adv. Funct. Mater.* **19**, 3420–3426 (2009)
- P. Yu, X. Zhang, D.L. Wang, L. Wang, Y.W. Ma, Shape-controlled synthesis of 3d hierarchical MnO₂ nanostructures for electrochemical supercapacitors. *Cryst. Growth Des.* **9**, 528–533 (2009)
- Y.B. Zhang, B. Wang, F. Liu, J.P. Cheng, X.W. Zhang, L. Zhang, Full synergistic contribution of electrodeposited three-dimensional NiCo₂O₄@MnO₂ nanosheet networks electrode for asymmetric supercapacitors. *Nano Energy* **27**, 627–637 (2016)
- G. Nagaraju, Y.H. Ko, S.M. Cha, S.H. Im, S.J. Yu, A facile one-step approach to hierarchically assembled core–shell-like MnO₂@MnO₂ nanoarchitectures on carbon fibers: an efficient and flexible electrode material to enhance energy storage. *Nano Res.* **9**, 1507–1522 (2016)
- M. Liu, W.W. Tjiu, J. Pan, C. Zhang, W. Gao, T. Liu, One-step synthesis of graphene nanoribbon-MnO₂ hybrids and their all-solid-state asymmetric supercapacitors. *Nanoscale* **6**, 4233–4242 (2014)
- D.W. Liu, Q.F. Zhang, P. Xiao, B.B. Garcia, Q. Guo, R. Champion, G.Z. Cao, Hydrous manganese dioxide nanowall arrays growth and their Li⁺ ions intercalation electrochemical properties. *Chem. Mater.* **20**, 1376–1380 (2008)
- V. Subramanian, H. Zhu, R. Vajtai, P.M. Ajayan, B. Wei, Hydrothermal synthesis and pseudocapacitance properties of MnO₂ nanostructures. *J. Phys. Chem. B* **109**, 20207–20214 (2005)

29. T. Yousefi, R. Davarkhah, A.N. Golikand, M.H. Mashhadizadeh, Synthesis, characterization, and supercapacitor studies of manganese (IV) oxide nanowires. *Mater. Sci. Semicond. Process* **16**, 868–876 (2013)
30. T. Yousefi, A.N. Golikand, M.H. Mashhadizadeh, M. Aghazadeh, Template-free synthesis of MnO₂ nanowires with secondary flower like structure: Characterization and supercapacitor behavior studies. *Curr. Appl. Phys.* **12**, 193–198 (2012)
31. W.H. Guo, T.J. Liu, P. Jiang, Z.J. Zhang, Free-standing porous manganese dioxide/graphene composite films for high performance supercapacitors. *J. Colloid Interface Sci.* **437**, 304–310 (2015)
32. H. Xia, Y. Wang, J.Y. Lin, L. Lu, Hydrothermal synthesis of MnO₂/CNT nanocomposite with a CNT core/porous MnO₂ sheath hierarchy architecture for supercapacitors. *Nanoscale Res. Lett.* **7**, 1–10 (2012)
33. G. Zhu, L. Deng, J. Wang, L. Kang, Z.-H. Liu, Hydrothermal preparation and the capacitance of hierarchical MnO₂ nanoflower. *Colloids Surf. A* **434**, 42–48 (2013)
34. Y.X. Wang, H.Q. Sun, H.M. Ang, M.O. Tade, S.B. Wang, 3D-hierarchically structured MnO₂ for catalytic oxidation of phenol solutions by activation of peroxymonosulfate: structure dependence and mechanism. *Appl Catal B Environ.* **164**, 159–167 (2015)
35. X.-H. Xia, J.-P. Tu, X.-L. Wang, C.-D. Gu, X.-B. Zhao, Hierarchically porous NiO film grown by chemical bath deposition via a colloidal crystal template as an electrochemical pseudocapacitor material. *J. Mater. Chem.* **21**, 671–679 (2011)
36. S.-C. Pang, M.A. Anderson, T.W. Chapman, Novel electrode materials for thin-film ultracapacitors: comparison of electrochemical properties of sol-gel-derived and electrodeposited manganese dioxide. *J. Electrochem. Soc.* **147**, 444 (2000)
37. N. Subramanian, B. Viswanathan, T.K. Varadarajan, A facile, morphology-controlled synthesis of potassium-containing manganese oxide nanostructures for electrochemical supercapacitor application. *RSC Adv.* **4**, 33911 (2014)
38. Q. Zhao, X. Wang, J. Liu, H. Wang, Y. Zhang, J. Gao, J. Liu, Q. Lu, Surface modification and performance enhancement of carbon derived from chromium carbide for supercapacitor applications. *J. Electrochem. Soc.* **162**, A845–A851 (2015)
39. J. Zhang, J. Zang, J. Huang, Y. Wang, G. Xin, Synthesis of an architectural electrode based on manganese oxide and carbon nanotubes for flexible supercapacitors. *Mater. Lett.* **126**, 24–27 (2014)
40. C.-C. Hu, C.-C. Wang, Nanostructures and capacitive characteristics of hydrous manganese oxide prepared by electrochemical deposition. *J. Electrochem. Soc.* **150**, A1079 (2003)
41. K. Liang, X. Tang, W. Hu, High-performance three-dimensional nanoporous NiO film as a supercapacitor electrode. *J. Mater. Chem.* **22**, 11062 (2012)
42. M. Huang, X.L. Zhao, F. Li, L.L. Zhang, Y.X. Zhang, Facile synthesis of ultrathin manganese dioxide nanosheets arrays on nickel foam as advanced binder-free supercapacitor electrodes. *J. Power Source* **277**, 36–43 (2015)
43. K. Qiu, Y. Lu, D. Zhang, J. Cheng, H. Yan, J. Xu, X. Liu, J.-K. Kim, Y. Luo, Mesoporous, hierarchical core/shell structured ZnCo₂O₄/MnO₂ nanocone forests for high-performance supercapacitors. *Nano Energy* **11**, 687–696 (2015)
44. C.J. Hung, P. Lin, T.Y. Tseng, High energy density asymmetric pseudocapacitors fabricated by graphene/carbon nanotube/MnO₂ plus carbon nanotubes nanocomposites electrode. *J. Power Source* **259**, 145–153 (2014)
45. C. Yuan, B. Gao, L. Su, X. Zhang, Interface synthesis of mesoporous MnO₂ and its electrochemical capacitive behaviors. *J. Colloid Interface Sci.* **322**, 545–550 (2008)
46. S.Z. Li, J. Wen, X.M. Mo, H. Long, H.N. Wang, J.B. Wang, G.J. Fang, Three-dimensional MnO₂ nanowire/ZnO nanorod arrays hybrid nanostructure for high-performance and flexible supercapacitor electrode. *J. Power Source* **256**, 206–211 (2014)
47. S.K. Meher, P. Justin, G.R. Rao, Pine-cone morphology and pseudocapacitive behavior of nanoporous nickel oxide. *Electrochim. Acta* **55**, 8388–8396 (2010)
48. C. Liu, F. Li, L.P. Ma, H.M. Cheng, Advanced materials for energy storage. *Adv Mater.* **22**, E28–E62 (2010)
49. P. Tang, L. Han, L. Zhang, Facile synthesis of graphite/PE/MnO₂ composites on commercial supercapacitor separator membranes as flexible and high-performance supercapacitor electrodes. *ACS Appl. Mater Interfaces* **6**, 10506–10515 (2014)
50. M. Kim, Y. Hwang, J. Kim, Fabrication of graphene-carbon nanotube papers decorated with manganese oxide nanoneedles on the graphene sheets for supercapacitors. *Phys. Chem. Chem. Phys.* **16**, 351–361 (2014)
51. P. Tang, L. Han, L. Zhang, S. Wang, W. Feng, G. Xu, L. Zhang, Controlled construction of hierarchical nanocomposites consisting of MnO₂ and PE for high-performance supercapacitor applications. *Chem. Electro. Chem.* **2**, 949–957 (2015)
52. Y. Li, Z.-Y. Fu, B.-L. Su, Hierarchically structured porous materials for energy conversion and storage. *Adv. Funct. Mater.* **22**, 4634–4667 (2012)